ELSEVIER

Transient growth for streak-streamwise vortex interactions

Lina Kim, Jeff Moehlis [*]

Department of Mechanical Engineering, University of California, Santa Barbara, CA 93106, USA

Abstract

We analyze transient growth due to the linear interaction between streaks and streamwise vortices. We obtain initial perturbations which give optimal initial and total energy growth, characterize the dependence of the dynamics on the initial distribution of perturbation energy, and compare with results from pseudospectra analysis.

© 2006 Elsevier B.V. All rights reserved.

1. Introduction

Shear flows are fluid flows which are non-homogeneous with a mean shear. Turbulent shear flows are of great fundamental physical and mathematical interest because [3]: (i) Turbulence is found both experimentally and in numerical simulations for values of the Reynolds number well below the value at which the laminar state loses stability [1], and (ii) the governing partial differential equations possess numerous branches of (unstable) steady or traveling states consisting of wavy streamwise vortices and streaks that arise in saddle-node bifurcations [4–7]. Such solutions have recently been detected experimentally [3, 8], but their relevance to turbulence remains unclear.

It has been suggested that transient energy growth provides a good basis for understanding property (i) (e.g. [2,23]). Such transient growth can significantly amplify small perturbations to the laminar state which can trigger non-linear effects that lead to sustained turbulence via the self-sustaining process identified in [12,13]. In this Letter, we analyze transient growth due to the linear interaction of the streak and streamwise vortex modes from the nine-mode model from [10,14]. This is a model

for sinusoidal shear flow, which obeys the non-dimensional equations

$$\frac{\partial \mathbf{u}}{\partial t} = -(\mathbf{u} \cdot \nabla)\mathbf{u} - \nabla p + \frac{1}{Re}\nabla^2 \mathbf{u} + \mathbf{F}(y),$$
$$\nabla \cdot \mathbf{u} = 0, \tag{1}$$

where the Reynolds number and body force are defined as

$$Re = \frac{U_0 d}{2\nu}, \qquad \mathbf{F}(y) = \frac{\sqrt{2}\pi^2}{4Re}\sin(\pi y/2)\hat{\mathbf{e}}_x, \tag{2}$$

U_0 is the characteristic velocity and ν is the kinematic viscosity. The free-slip boundary conditions

$$u_y = 0, \qquad \frac{\partial u_x}{\partial y} = \frac{\partial u_z}{\partial y} = 0 \tag{3}$$

are imposed at $y = \pm 1$, and the flow is assumed periodic in the streamwise (x) and spanwise (z) directions, with lengths L_x and L_z, respectively. The laminar profile for sinusoidal shear flow,

$$\mathbf{U}(y) = \sqrt{2}\sin(\pi y/2)\hat{\mathbf{e}}_x \tag{4}$$

is linearly stable for all Re [1]. In the following, we let $\alpha = 2\pi/L_x$, $\beta = \pi/2$, and $\gamma = 2\pi/L_z$. Although difficult to obtain experimentally, sinusoidal shear flow represents a non-trivial shear flow which is amenable to analytical treatment; it is hoped that the knowledge gained from the present analysis will be

[*] Corresponding author. Tel.: +1 805 893 7513; fax: +1 805 893 8651.

E-mail addresses: lina@engineering.ucsb.edu (L. Kim),
moehlis@engineering.ucsb.edu (J. Moehlis).

helpful for characterizing other shear flows such as plane Couette flow, boundary layer flow, Poiseuille flow, and pipe flow.

In Section 2, a geometric interpretation of transient growth due to the interaction between streaks and streamwise vortices is given. Then, the details of how such transient growth depends on initial conditions, *Re*, and aspect ratio are derived. Furthermore, the neutral transient growth curve, below which *no* initial condition gives transient energy growth, is found and discussed. In Section 3, the transient energy growth is interpreted using pseudospectra analysis, where a lower bound for the maximum attainable energy is obtained using Kreiss' theorem. We will see that the analysis in Section 2 gives a sharper characterization of the transient growth than that in Section 3. Our conclusions are given in Section 4.

2. Transient growth for the streak-streamwise vortex interaction

The matrix M arising from the linearization of the nine-mode model from [10] about the laminar state is non-normal, i.e., $MM^T \neq M^T M$. This suggests that even though its eigenvalues are all strictly negative for all *Re*, corresponding to linear stability of the laminar state, it might be possible to have transient growth of energy which could trigger non-linear effects that sustain turbulence [2,25]. In this section, a detailed analysis is conducted for the transient growth which occurs for the 2×2 block of M that corresponds to the linear evolution of the amplitudes a_2 and a_3, which give the amplitudes of the streamwise invariant streak and streamwise vortex modes

$$
\mathbf{u}_2 = \begin{pmatrix} \frac{4}{\sqrt{3}} \cos^2(\pi y/2) \cos(\gamma z) \\ 0 \\ 0 \end{pmatrix},
$$

$$
\mathbf{u}_3 = \frac{2}{\sqrt{4\gamma^2 + \pi^2}} \begin{pmatrix} 0 \\ 2\gamma \cos(\pi y/2) \cos(\gamma z) \\ \pi \sin(\pi y/2) \sin(\gamma z) \end{pmatrix}, \quad (5)
$$

respectively. We focus on this interaction because it gives the strongest transient energy growth compared to the other interactions of the linearized nine-dimensional model. Furthermore, streaks and streamwise vortices are dominant structures in numerical simulations and are related to unstable steady solutions of the Navier–Stokes equations [4–6,9]. Finally, they are related to optimal perturbations [17] and are the most energetically excited structures of the linearized Navier–Stokes equations with forced input and can be explained as input–output resonances of frequency responses [19].

A Galerkin projection onto these modes gives the linear system

$$
\begin{pmatrix} \dot{a}_2 \\ \dot{a}_3 \end{pmatrix} = \underbrace{\begin{pmatrix} b & c \\ 0 & d \end{pmatrix}}_{M_{23}} \begin{pmatrix} a_2 \\ a_3 \end{pmatrix}, \quad (6)
$$

$$
b = -\frac{\frac{4\beta^2}{3} + \gamma^2}{Re} = \mathcal{O}(Re^{-1}), \qquad c = -\frac{\sqrt{3/2}\beta\gamma}{\sqrt{\beta^2 + \gamma^2}} = \mathcal{O}(Re^0),
$$

$$
d = -\frac{\beta^2 + \gamma^2}{Re} = \mathcal{O}(Re^{-1}). \quad (7)
$$

Here and elsewhere we give the scaling behavior for large *Re*. The laminar state corresponds to $a_2 = a_3 = 0$; the stability of the laminar state with respect to streak and streamwise vortex perturbations follows from the fact that the eigenvalues b and d of M_{23} are negative. The exact solution to (6) is readily shown to be

$$
a_2(t) = a_{20}e^{bt} + \frac{c}{d-b}a_{30}(e^{dt} - e^{bt}), \quad a_3(t) = a_{30}e^{dt}. \quad (8)
$$

For this system, the energy is defined to be $E(t) = (a_2(t))^2 + (a_3(t))^2$. We note that (6) also arises in the linearization of the eight-mode model from [13] and the uncoupled-mode model from [15] about the laminar state, with the same *Re* dependence of b, c, d but with different values.

2.1. Geometric interpretation of transient energy growth

The solution (8) can be rewritten in a form which allows an instructive geometric interpretation of transient energy growth, namely

$$
\mathbf{a}(t) = (a_2(t), a_3(t)) = \underbrace{\mathbf{v}_1 b_{10}e^{bt}}_{\mathbf{s}_1(t)} + \underbrace{\mathbf{v}_2 b_{20}e^{dt}}_{\mathbf{s}_2(t)}, \quad (9)
$$

where formulas for b_{10} and b_{20} in terms of a_{20} and a_{30} are readily obtained, and $\mathbf{v}_1$ and $\mathbf{v}_2$ are the normalized eigenvectors for M_{23}. Since M_{23} is non-normal, $\mathbf{v}_1$ and $\mathbf{v}_2$ are non-orthogonal; for example, for the values $L_z = 1.2\pi$ and $Re = 400$ studied below, they are almost anti-parallel. For the related system of plane Couette flow, these parameters correspond to the minimal flow unit, the smallest domain which is found numerically to sustain turbulence [16]. A small-amplitude initial condition is thus the superposition of two very large-amplitude components; i.e., $|\mathbf{s}_1(0)|$ and $|\mathbf{s}_2(0)|$ are large, as sketched in the left panels of Fig. 1. For the linear system, $b < d < 0$, so the length of $\mathbf{s}_1(t)$ decays more quickly than the length of $\mathbf{s}_2(t)$. This leads to an $\mathbf{a}(t)$ with larger length (and hence larger energy) than $\mathbf{a}(0)$, as sketched in the right panel of Fig. 1(a); thus, transient growth has occurred. For longer times, the length of $\mathbf{s}_2(t)$ also decreases substantially, and the system asymptotically approaches the laminar state with $a_2 = a_3 = 0$.

For other initial conditions, transient energy growth might not occur: see Fig. 1(b). Clearly, the energy initially decreases with time. Depending on the rate of decay of the length of $\mathbf{s}_2(t)$, the energy might always remain below its initial value, or might eventually grow above its initial value. Such considerations motivate the following exploration of how transient energy growth depends on initial conditions.

2.2. Application to the streak-streamwise vortex interaction

A general linear equation $\dot{\mathbf{a}} = A\mathbf{a}$ has the exact solution $\mathbf{a}(t) = e^{tA}\mathbf{a}_0$, where $\mathbf{a}_0 = \mathbf{a}(0)$. The energy of a solution is defined as $E(t) = |\mathbf{a}(t)|^2 = \sum a_i^2$, where the sum is over the components of $\mathbf{a}$. It is found that $E'(0) = 2\mathbf{a}_0 \cdot A\mathbf{a}_0 \equiv f(\mathbf{a}_0)$. To find the (normalized) initial condition which gives the maximum initial energy growth, $f(\mathbf{a}_0)$ is maximized subject to the constraint $g(\mathbf{a}_0) \equiv |\mathbf{a}_0|^2 = 1$. Using a Lagrange multiplier λ to
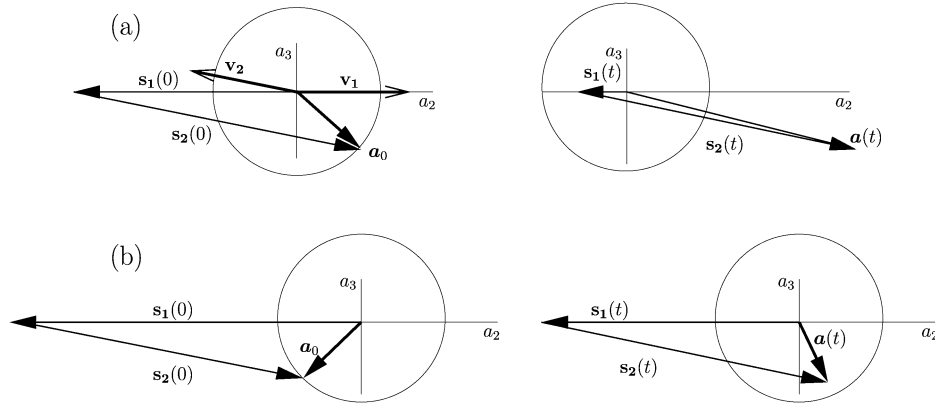
Fig. 1. Geometric interpretation of transient growth. The circles represent constant energy equal to the initial energy. Because $\mathbf{v}_1$ and $\mathbf{v}_2$ are nearly anti-parallel, the initial condition is $\boldsymbol{a}_0 = \mathbf{s}_1(0) + \mathbf{s}_2(0)$ with large $|\mathbf{s}_1(0)|$ and $|\mathbf{s}_2(0)|$, as shown in the left panels of (a) and (b). Because of different decay rates, in the right panels $|\mathbf{s}_1(t)| < |\mathbf{s}_2(t)| \approx |\mathbf{s}_2(0)|$. In (a), $|\boldsymbol{a}(t)| > |\boldsymbol{a}_0|$ for short times, so that transient growth occurs. In (b), $|\boldsymbol{a}(t)| < |\boldsymbol{a}_0|$, so that transient growth does not occur, at least for short times. For clarity, the difference in decay rates is assumed to be large for this figure.

impose this constraint, we obtain $(A + A^T)\boldsymbol{a}_0 = \lambda \boldsymbol{a}_0$. Thus the eigenvalues and eigenvectors of $A + A^T$ need to be found. It is also readily shown that $\boldsymbol{a}_0 \cdot A\boldsymbol{a}_0 = \boldsymbol{a}_0 \cdot A^T \boldsymbol{a}_0$, which gives

$$E'(0) = \boldsymbol{a}_0 \cdot \left(A + A^T \right) \boldsymbol{a}_0 = \lambda |\boldsymbol{a}_0|^2. \tag{10}$$

Therefore, the largest (respectively, smallest) value that $E'(0)$ can obtain, when $E(0) = |\boldsymbol{a}_0|^2 = 1$, is equal to the largest (respectively, smallest) eigenvalue of the matrix $A + A^T$. The initial condition that maximizes (respectively, minimizes) the initial energy growth is the corresponding eigenvector of this matrix (cf. [11]).

For the present problem, we take $A = M_{23}$. The maximum value that $E'(0)$ can take is the larger eigenvalue of $M_{23} + M_{23}^T$:

$$\left[E'(0) \right]_{\max} = b + d + \sqrt{b^2 + c^2 - 2bd + d^2}, \tag{11}$$

with corresponding (unnormalized) eigenvector

$$(a_{20}, a_{30}) = \left(\frac{d - b - \sqrt{b^2 + c^2 - 2bd + d^2}}{c}, -1 \right). \tag{12}$$

For large Re, $b \to 0$ and $d \to 0$, so we find that $[E'(0)]_{\max} \approx |c| = \mathcal{O}(Re^0)$, and the corresponding (normalized) eigenvector which maximizes $E'(0)$ is $(a_{20}, a_{30}) = (1/\sqrt{2}, -1/\sqrt{2})$. This corresponds to the initial energy being equally distributed between the streaks and the streamwise vortices; as will be shown below, the phases between these modes are such that the advection of fluid by the streamwise vortices reinforces the streaks.

The initial rate of energy growth $E'(0)$ clearly depends on the initial distribution of energy between the streamwise vortices and the streaks. Let $E(0) = a_{20}^2 + a_{30}^2 = 1$, and $\theta = \tan^{-1}(a_{30}/a_{20})$, where $\theta = 0$ corresponds to the initial energy being entirely in the streaks. Differentiating $E(t)$ and using (6) gives

$$E'(0) = b + d + (b - d)\cos 2\theta + c \sin 2\theta. \tag{13}$$

This is periodic with period π because rotation of θ by π corresponds to multiplication of a_{20} and a_{30} by -1, which has only a trivial effect for a linear problem. For large Re, $E'(0) \approx c \sin 2\theta = \mathcal{O}(Re^0)$. $E'(0)$ reaches its maximum value

of $|c|$ for $\theta \approx 3\pi/4$ and $\theta \approx 7\pi/4$, and its minimum value of $-|c|$ for $\theta \approx \pi/4$ and $\theta \approx 5\pi/4$ (recall that $c < 0$). These results demonstrate how different initial distributions of energy affect the transient dynamics of the system.

Progress can also be made in understanding how the maximum value that $E(t)$ reaches under the linear evolution depends on the initial distribution of energy between streamwise vortices and streaks, as captured by θ. In the limit of large Re, from (8) and using $E(0) = a_{20}^2 + a_{30}^2 = 1$,

$$E(t) = \left[a_2(t) \right]^2 + \left[a_3(t) \right]^2 \approx \left(\frac{c}{d - b} \right)^2 \left(e^{dt} - e^{bt} \right)^2 \sin^2 \theta. \tag{14}$$

The above also requires that θ is not too close to 0 or π, so that the first term of $a_2(t)$ in (8) has a small magnitude relative to the second term. By solving $E'(t) = 0$ for t using (14), $E(t)$ reaches its maximum at

$$t_{\max E} \approx \frac{\log(d/b)}{b - d} = \mathcal{O}(Re), \tag{15}$$

with

$$\begin{aligned} E_{\max} &\approx E(t_{\max E}) \\ &\approx \left(\frac{c}{d - b} \right)^2 \\ &\quad \times \left(b^{b/(d-b)} d^{b/(b-d)} - b^{d/(d-b)} d^{d(b-d)} \right)^2 \sin^2 \theta \\ &= \mathcal{O}\left(Re^2 \right). \end{aligned} \tag{16}$$

The absolute maximum energy that can occur for the linear dynamics of the modes for streaks and streamwise vortices, for large fixed Re, thus occurs for $\theta \approx \pi/2$ and $\theta \approx 3\pi/2$. This corresponds to the initial energy being entirely in the streamwise vortices. Note that the initial conditions which maximize $E'(0)$ give $\sin^2 \theta = 1/2$, so that for large Re the absolute maximum energy is double the maximum energy obtained for the initial condition which maximizes initial energy growth. Furthermore, note that when θ is sufficiently close to 0 or π, the approximations (14) and (16) are not valid, and $E_{\max} = E(0)$. For example, $\theta = 0$ implies that $a_{30} = 0$, and that $E(t) = a_{20}^2 e^{2bt}$ is monotonically decreasing.
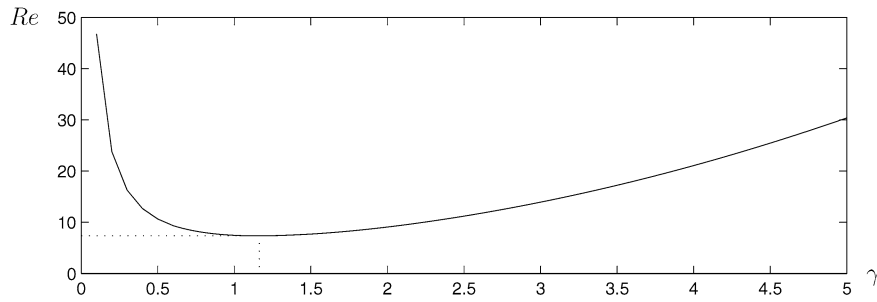
Fig. 2. Neutral transient growth curve $Re^*(\gamma)$. Above this curve, $E'(0) > 0$ for some initial distribution of energy as captured by θ. Below this curve, there are no such θ values. As discussed in the text, above this curve it is also possible to find an initial condition for which $E(t) > E(0)$ for some $t > 0$, while below this curve there is no such initial condition.

2.3. Neutral transient growth

As just shown, initial conditions have a dramatic effect on transient energy growth. A neutral transient growth curve, below which *no* initial condition gives transient energy growth, can be found by solving $[E'(0)]_{max}$ for Re from (11). Using (7), this gives the curve

$$Re^*(\gamma) = \frac{2\sqrt{2(\beta^2 + \gamma^2)^2(4\beta^2 + 3\gamma^2)}}{3\beta\gamma}, \qquad (17)$$

see Fig. 2. For a given aspect ratio γ, for $Re > Re^*(\gamma)$ it is possible to find an initial condition with initial transient energy growth, while for $Re < Re^*(\gamma)$ there are no such initial conditions. It is found that $Re^*(\gamma)$ reaches a minimum at $\gamma^* = 1.1634$ with $Re^*(\gamma^*) = 7.3573$. For $Re < Re^*(\gamma^*)$, there are no possible initial conditions for which $E'(0) > 0$. For $Re > Re^*(\gamma^*)$, there will be a band of θ values for which $E'(0) > 0$. There is a *larger* band of initial θ values for which $E(t) > E(0)$ for some $t > 0$, that is, for which the energy eventually exceeds its initial value. As detailed in [22], for a given γ and Re, the boundary of this band is readily found by numerically finding the roots of an appropriate equation.

Interestingly, the curve for $Re^*(\gamma)$ given by (17) coincides with the curve above which it is possible to find an initial condition for which $E(t) > E(0)$ for some $t > 0$, and below which there is no such initial condition. Without loss of generality, take $E(0) = 1$. Certainly this new curve cannot lie above the curve for $Re^*(\gamma)$, because $E'(0) > 0$ for some θ guarantees that $E(t) > E(0)$ for some $t > 0$ for that initial condition. Instead, suppose that one chooses $Re < Re^*(\gamma^*)$, so that for all θ values $E'(0) < 0$. If there is a t_1 such that $E(t_1) = E(0) = 1$ and $E'(t_1) > 0$, then $E(t) > E(0)$ for some $t > t_1 > 0$. Now, at time t_1 the solution has unit energy, and corresponds to some value for θ. If the initial θ value was taken to be this, then it would result in $E'(0) > 0$. This contradicts the assumption that $E'(0) < 0$ for all θ values. Therefore, the new curve cannot lie below the curve for $Re^*(\gamma)$, so they must coincide.

For a very large aspect ratio system, the curve $Re^*(\gamma)$ is defined to be the neutral transient growth curve, much in the spirit of neutral stability curves for standard hydrodynamic stability analysis: for fixed aspect ratio, it defines the value of Re at which transient growth is possible, while for fixed Re it defines the range of wavenumbers γ for which transient growth is possible.

2.4. Results for $L_z = 1.2\pi$

As a representative example, consider the aspect ratio $L_z = 1.2\pi$. For $Re = 400$, it was found that the unit energy initial condition $(a_2(0), a_3(0)) = (0.7066, -0.7076)$ gives $[E'(0)]_{max} = 1.3717$; the large Re prediction is 1.4000. This is the initial condition which gives the maximum initial energy growth, corresponding to an approximately equal distribution of initial energy between the streaks and streamwise vortices. The *absolute* maximum energy which can be obtained for the linear dynamics with unit energy initial condition occurs for $(a_2(0), a_3(0)) \approx (0, -1)$. This initial condition corresponds to the initial energy being entirely in the streamwise vortices and gives $t_{max\,E} = 70.83$ and $E_{max} = 1329.03$, which agree well with the predictions from (15) and (16). Figs. 3 and 4 show the velocity fields and $a_2(t), a_3(t)$, and $E(t)$ for both initial conditions, respectively. The vortices advect the fluid as to strengthen the streaks and since the energy in the streamwise vortices decays monotonically, the bulk of the energy for both perturbations, when it reaches its peak, is in the streaks. Clearly, it is possible to get substantial transient energy growth for this system which might trigger non-linear effects that lead to sustained turbulence via the self-sustaining process of [12,13], in which streamwise vortices cause streak formation, then streaks break down to give streamwise-dependent flow, then streamwise vortices regenerate and the process repeats. Finally, Fig. 5(a) shows boundaries of qualitatively different dynamics for $E(t)$ in terms of Re and θ. Fig. 5(b) shows the time series for $E(t)$ in each distinct region at $Re = 20$. For more details on calculating these curves see [22].

3. Pseudospectra analysis

An alternative method of analyzing a non-normal matrix is to calculate its pseudospectrum [20,21], which is a generalization of eigenvalue analysis. For $\epsilon > 0$, the ϵ-pseudospectrum of a matrix A is defined as

$$\Lambda_\epsilon(A) = \{z \in \mathbb{C}: \|(zI - A)^{-1}\|_2 \geqslant \epsilon^{-1}\}, \qquad (18)$$

with $\|\cdot\|_2$ representing the 2-norm. When z is an eigenvalue of A, it is useful to take the convention that $\|(zI - A)^{-1}\|_2$
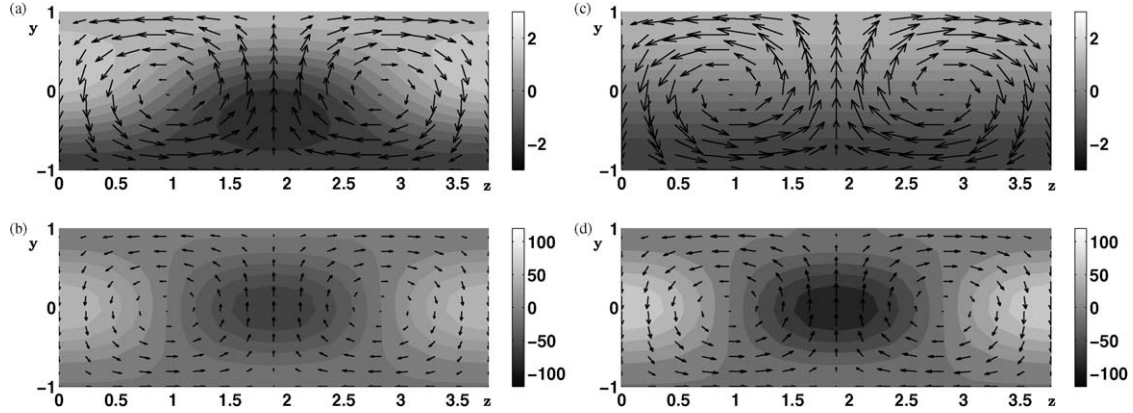
Fig. 3. Velocity fields for $L_z = 1.2\pi$, $Re = 400$, and (a) the initial condition which maximizes $E'(0)$, and (b) the state for this initial condition when E is maximized; (c) the initial condition which gives $E_{\max}$, the absolute maximum of E, and (d) the state for this initial condition when this $E_{\max}$ is obtained. The velocity fields are represented by vectors for the components shown in the plane and by grayscale for the velocity perpendicular to the plane. The vectors are identically scaled, so the shorter arrows in the bottom plot indicate weaker vortices. The laminar profile has been included in these plots.
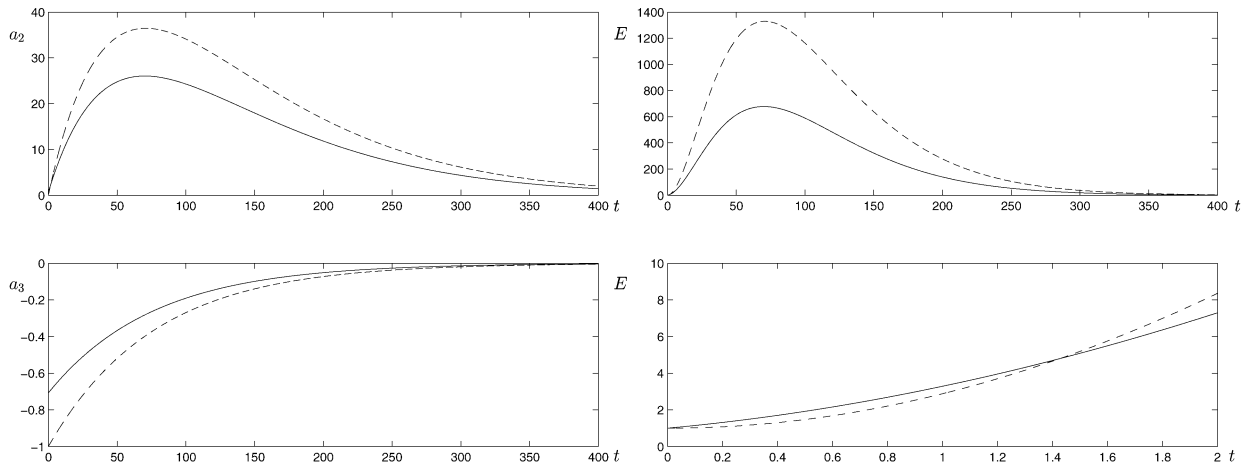

Fig. 4. Solution for (6) with $L_z = 1.2\pi$, and $Re = 400$ for the initial condition which gives the maximum initial energy growth $E'_{\max}(0)$ (solid lines) and the initial condition which gives the absolute maximum energy $E_{\max}$ which can occur (dashed lines).

is infinite. Thus, the eigenvalues are given by $\Lambda_0(A)$. The ϵ-pseudospectra are closed, and if $\epsilon_1 < \epsilon_2$, then $\Lambda_{\epsilon_1} \subset \Lambda_{\epsilon_2}$.

An equivalent definition of the pseudospectrum is that $\Lambda_\epsilon(A)$ is the set of all complex numbers z for which the smallest singular value of $L \equiv zI - A$ is less than or equal to ϵ. This follows from the above definition and the fact that the 2-norm of $(zI - A)^{-1}$ equals the smallest singular value of $zI - A = L$. The boundary of the ϵ-pseudospectrum $\Lambda_\epsilon(A)$ is then found by setting the smallest singular value of L equal to ϵ. Recall that the singular values of L are the square roots of the eigenvalues of $LL^\dagger$, with the 2-norm of L being equal to its largest singular value.

Here, we let $A = M_{23}$, and therefore the ϵ-pseudospectra can be found exactly from the definition

$$
\begin{aligned}
L &= zI - M_{23} \\
&= \begin{pmatrix} z - b & -c \\ 0 & z - d \end{pmatrix} = \begin{pmatrix} X + iY - b & -c \\ 0 & X + iY - d \end{pmatrix},
\end{aligned} \quad (19)
$$

where $z = X + iY$. The boundary of $\Lambda_\epsilon(A)$ is found by setting the square root of the smallest eigenvalue of $LL^\dagger$ equal to ϵ. Kreiss' theorem uses pseudospectra to obtain a lower bound for

the maximum attainable energy [20]:

$$
\max_{t>0} \| e^{At} \|_2^2 \geqslant \left[\sup_{\epsilon>0} \frac{\delta(\epsilon)}{\epsilon} \right]^2, \quad (20)
$$

where the left-hand side is the maximum attainable energy given a unit energy initial condition, and

$$
\delta(\epsilon) = \sup_{\substack{\mathbb{R}(z)>0 \\ z \in \Lambda_\epsilon(A)}} (\mathbb{R}(z)), \quad (21)
$$

that is, $\delta(\epsilon)$ is the largest distance from the imaginary axis to a point in the unstable half-plane lying within the ϵ-pseudospectrum contour. See [20,22] for a detailed derivation.

3.1. Results for $L_z = 1.2\pi$

For $L_z = 1.2\pi$, $Re = 10$, the eigenvalues of M_{23} are $b = -0.6068$ and $d = -0.5245$. For small values of ϵ, the boundary of $\Lambda_\epsilon(M_{23})$ is disconnected, with separate components surrounding each eigenvalue individually; for larger values of ϵ, the boundary encloses both eigenvalues; see Fig. 6(a). To find a
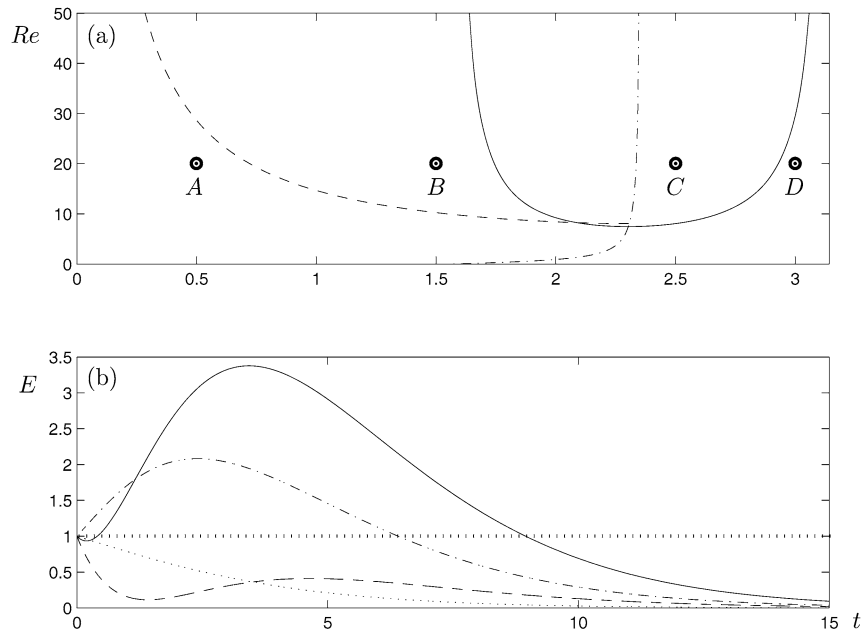
Fig. 5. Boundaries of qualitatively different $E(t)$ for $L_z = 1.2\pi$. (a) The θ values inside the solid curve correspond to initial conditions for which $E'(0) > 0$. The θ values to the right of the dashed curve and to the left of the right branch of the solid curve correspond to initial conditions for which $E(t) > E(0)$ for some $t > 0$. The dot-dashed line shows the initial condition giving $[E'(0)]_{max}$. (b) The points A, B, C, D give the qualitatively distinct behaviors shown in the lower plot describing time evolution of energy for $Re = 20$ and $E(0) = 1$ for (A) $\theta = 0.5$ (dashed), (B) $\theta = 1.5$ (solid), (C) $\theta = 2.5$ (dot-dashed), and (D) $\theta = 3$ (dotted).
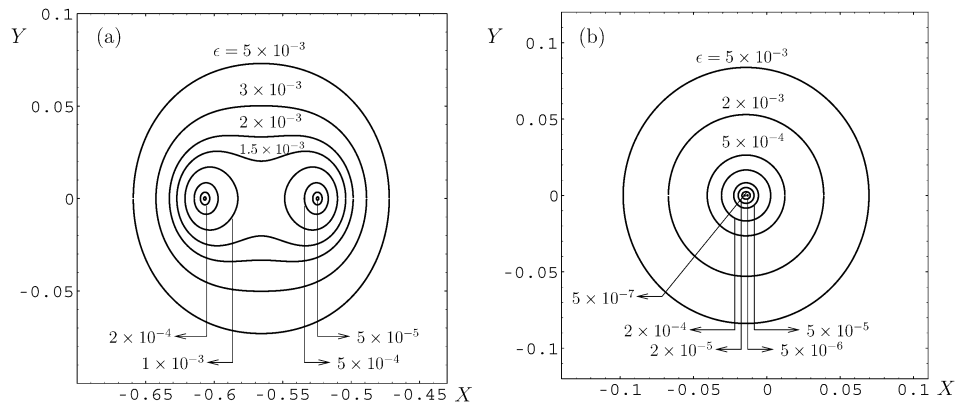

Fig. 6. Boundaries for pseudospectra for $L_z = 1.2\pi$ with (a) $Re = 10$ and (b) $Re = 400$, with ϵ values as labeled.
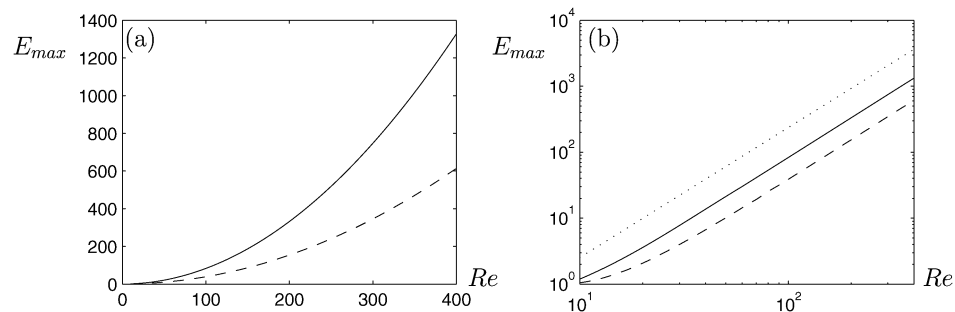

Fig. 7. (a) Comparison of E_{max} (solid) to lower bound (dashed) for variable Re values and $L_z = 1.2\pi$. (b) shows the same results as (a) but using logarithmic axes. The dotted line in (b) has slope equal to 2.

lower bound for E_{max}, the ratio of $\delta(\epsilon)$ to ϵ was calculated as a function of ϵ and was found to be maximized for $\epsilon = 2.6$, yielding a lower bound which is close to the numerically-obtained absolute maximum energy of E_{max}.

Keeping $L_z = 1.2\pi$ but for $Re = 400$, the eigenvalues are much closer to one another, with $b = -0.0152$, and $d = -0.0131$. This means that extremely small ϵ values, on the order of 10^{-8}, are needed to give boundaries which surround each eigenvalue individually; see Fig. 6(b). As above, a lower bound for E_{max} can be calculated. Here, $\epsilon = 5.8 \times 10^{-4}$ which gives a lower bound for the maximum attainable energy of 613.70, which is approximately half the numerically-obtained value of E_{max}. Fig. 7 shows the relationship between E_{max} and the lower bound obtained using Kreiss' theorem as a function of Re. The lower bound becomes less sharp as Re increases, but both the absolute maximum attainable energy and the lower bound scale as Re^2, the former being expected from (16); see Fig. 7(b). These results show that although pseudospectra is an important tool for studying non-normal matrices, it may not provide the sharpest results.

4. Conclusion

We have analyzed transient growth due to the linear interaction between streaks and streamwise vortices. It was shown that it is possible to get substantial transient growth before the system decays to the laminar state and how the magnitude of growth depends on initial conditions, Re, and aspect ratio. For large Re, it was found that the maximum energy obtained for the initial condition which maximizes initial energy growth, which corresponds to an equal initial energy distribution between the streaks and streamwise vortices, is half the absolute maximum energy, which is obtained when the initial energy is entirely in the streamwise vortices. Furthermore, a neutral transient growth curve, below which *no* initial condition gives transient growth was found. The results were compared with an alternative interpretation of transient growth using pseudospectra, which gives to a lower bound for the maximum attainable energy. Our analysis allowed for a sharper characterization of transient growth than can be obtained from pseudospectra.

It is worth emphasizing that these results provide much more insight into the dynamics of this interaction than standard stability analysis, which just calculates eigenvalues, and hence only captures asymptotic behavior. Furthermore, the standard analysis would not identify key differences in the situation, for example, in which there is an equal initial distribution of energy between streaks and rolls, or when the energy is all initially in the streamwise vortices. The analysis in this Letter overcomes these limitations by usefully capturing the transient behavior and the importance of different initial distributions of energy.

The results show that the linear dynamics of the streaks and streamwise vortices can lead to substantial transient growth and are consistent with previous results for plane Couette flow [17] and Taylor–Couette flow [18,24]. The approach presented in this Letter has the advantage of exploring how the results depend on the aspect ratio, Reynolds number, and initial conditions. An investigation into the role of transient growth for triggering non-linear interactions and the transition to turbulence, in the context of the full nonlinear nine-dimensional model of [10], is currently in progress.

References

[1] P.G. Drazin, W.H. Reid, Hydrodynamic Stability, Cambridge Univ. Press, Cambridge, 1981.
[2] L.N. Trefethen, A.E. Trefethen, S.C. Reddy, T.A. Driscoll, Science 261 (1993) 578.
[3] F.H. Busse, Science 305 (2004) 1574.
[4] M. Nagata, J. Fluid Mech. 217 (1990) 519.
[5] R.M. Clever, F.H. Busse, J. Fluid Mech. 234 (1992) 511.
[6] A. Schmiegel, Transition to turbulence in linearly stable shear flows, Ph.D. thesis, Universität Marburg, Marburg, Germany, 1999.
[7] H. Faisst, Turbulence transition in pipe flow, Ph.D. thesis, Universität Marburg, Marburg, Germany, 2003.
[8] B. Hof, C.W.H. van Doorne, J. Westerweel, F.T.M. Nieuwstadt, H. Faisst, B. Eckhardt, H. Wedin, R.R. Kerswell, F. Waleffe, Science 305 (2004) 1594.
[9] J. Moehlis, T.R. Smith, P. Holmes, H. Faisst, Phys. Fluids 14 (2002) 2493.
[10] J. Moehlis, H. Faisst, B. Eckhardt, New J. Phys. 6 (2004), article 56.
[11] J.S. Baggett, L.N. Trefethen, Phys. Fluids 9 (1997) 1043.
[12] F. Waleffe, Phys. Fluids 7 (1995) 3060.
[13] F. Waleffe, Phys. Fluids 9 (1997) 883.
[14] J. Moehlis, H. Faisst, B. Eckhardt, SIAM J. Appl. Dyn. Systems 4 (2005) 352.
[15] T.R. Smith, J. Moehlis, P. Holmes, J. Fluid Mech. 538 (2005) 71.
[16] J. Hamilton, J. Kim, F. Waleffe, J. Fluid Mech. 287 (1995) 317.
[17] K.M. Butler, B.F. Farrell, Phys. Fluids A 4 (1992) 1637.
[18] H. Hristova, S. Roch, P.J. Schmid, L.S. Tuckerman, Phys. Fluids 14 (2002) 3475.
[19] M.R. Jovanović, B. Bamieh, J. Fluid Mech. 543 (2005) 145.
[20] P.J. Schmid, D.S. Henningson, Stability and Transition in Shear Flows, Springer-Verlag, New York, 2000.
[21] L.N. Trefethen, Pseudospectra of Matrices, Numerical Analysis, vol. 1991, Longman Sci. Tech., Harlow, Essex, 1992.
[22] L. Kim, Transient growth for a sinusoidal shear flow model, M.S. thesis, University of California, Santa Barbara, 2005.
[23] S.J. Chapman, J. Fluid Mech. 451 (2002) 35.
[24] À. Meseguer, Phys. Fluids 14 (2002) 1655.
[25] D.S. Henningson, S.C. Reddy, Phys. Fluids 6 (1994) 1396.